Deletion of the de novo DNA methyltransferase *Dnmt3a* promotes lung tumor progression

Qing Gao[a], Eveline J. Steine[a], M. Inmaculada Barrasa[a], Dirk Hockemeyer[a], Mathias Pawlak[a], Dongdong Fu[a], Seshamma Reddy[a,1], George W. Bell[a], and Rudolf Jaenisch[a,b,2]

[a]Whitehead Institute for Biomedical Research, Cambridge, MA 02142; and [b]Department of Biology, Massachusetts Institute of Technology, Cambridge, MA 02139

Contributed by Rudolf Jaenisch, September 15, 2011 (sent for review July 29, 2011)

Alterations in DNA methylation have been associated with genome-wide hypomethylation and regional de novo methylation in numerous cancers. De novo methylation is mediated by the de novo methyltransferases Dnmt3a and 3b, but only Dnmt3b has been implicated in promoting cancer by silencing of tumor-suppressor genes. In this study, we have analyzed the role of Dnmt3a in lung cancer by using a conditional mouse tumor model. We show that Dnmt3a deficiency significantly promotes tumor growth and progression but not initiation. Changes in gene expression show that Dnmt3a deficiency affects key steps in cancer progression, such as angiogenesis, cell adhesion, and cell motion, consistent with accelerated and more malignant growth. Our results suggest that *Dnmt3a* may act like a tumor-suppressor gene in lung tumor progression and may be a critical determinant of lung cancer malignancy.

adenocarcinoma | cancer epigenetics | gene body methylation | *K-ras*

Changes in the DNA methylation status are among the most common molecular alterations in cancer (1, 2). Genome-wide hypomethylation and promoter hypermethylation are hallmarks of a great variety of cancers contributing to tumorigenesis. Global hypomethylation can result in increased genomic instability, reactivation of silenced parasitic genes, and loss of imprinting (3, 4), whereas hypermethylation of CpG islands in gene promoters can silence tumor-suppressor genes and affect critical cellular processes, such as cell-cycle control, apoptosis, DNA repair, cell–cell interaction, and angiogenesis (5).

The de novo methyltransferases Dnmt3a and Dnmt3b are highly expressed during early embryonic development and downregulated in most differentiated somatic cells (6). In human cancers, however, Dnmt3b is frequently overexpressed (7, 8), consistent with the notion that inappropriate expression of Dnmt3b may silence tumor-suppressor genes and thus contribute to tumorigenesis. Based upon tissue-specific gene deletion and induction, Dnmt3b has been identified in mouse models to carry out de novo methylation of genes that are typically silenced in human colon cancer and to promote intestinal tumor formation (9–11). In contrast to Dnmt3b, the role of Dnmt3a in cancer is far less understood. DNMT3A was found to be overexpressed in some human cancers (12) and in a mouse xenograft model, the knockdown of *Dnmt3a* was shown to suppress melanoma growth and metastasis (13). In contrast, induction of Dnmt3a in APC^{Min} mice had no effect on intestinal tumor formation (9). The role of DNMT3A in human cancer was highlighted by reports of *DNMT3A* mutations in approximately 20% of patients with acute myeloid leukemia (14, 15). The occurrence of these mutations correlated with reduced enzymatic activity and genomic regions with decreased methylation. *DNMT3A* mutations were also identified in 8% of patients with myelodysplastic syndrome (16). In all these reports, the *DNMT3A* mutations correlated with poor prognosis.

Lung cancer is the leading cause of cancer death in the United States (17) and can be divided into four types—adenocarcinoma (AD), squamous-cell carcinoma, large-cell carcinoma, and small-cell lung carcinoma—with AD being the most common type. Both genetic and epigenetic factor have been implicated in lung cancer. The mutation of *K-ras* is one of the most common genetic lesions and can be found in a large fraction of lung cancers. Promoter hypermethylation is perhaps the best characterized epigenetic aberration and can be used as a screening marker for early detection, prevention, and prognosis (18, 19).

In this study, we have established an experimental system to investigate the role of Dnmt3a in lung AD. We show that deletion of *Dnmt3a* in mutant *K-ras* induced lung tumors significantly promotes tumor progression, suggesting that this gene functions like a tumor suppressor.

Results

***Dnmt3a* Deletion Accelerates Tumor Growth.** To test the effect of *Dnmt3a* deletion on lung cancer, we generated mice carrying a conditional $K\text{-}ras^{LSL\text{-}G12D}$ allele (20) and 2Lox alleles of *Dnmt3a* (21) ($K\text{-}ras^{LSL\text{-}G12D}/Dnmt3a^{2Lox/2Lox}$) (Fig. 1*A*). Oncogene activation and *Dnmt3a* deletion were induced by intratracheal infusion with adenoviral Cre recombinase (Ad-Cre) (22).

The lungs of infected animals were removed and prepared for histologic examination at weeks 8, 16, and 24 after Ad-Cre administration. No significant differences in tumor number and size were seen in lungs of animals at week 8. In contrast, Dnmt3a-deficient (KO) and WT mice showed a dramatic difference at weeks 16 and 24 after infection. Whereas most tumors in lungs of Dnmt3a WT animals were small (as large as 0.2 cm in diameter), lungs of Dnmt3a-deficient mice were characterized by a significant increase in the number of large tumors (Fig. 1*B*). This was confirmed on histological sections of the lungs (Fig. 1*C*). As summarized in Fig. 1*D*, the average size of Dnmt3a-deficient tumors was approximately four times larger at week 16 and six times larger at week 24 compared with WT tumors. Similarly, the fraction of the total lung area occupied by Dnmt3a-deficient tumors was approximately four times larger than that occupied by WT tumors at weeks 16 and 24 (Fig. 1*E*). However, the total number of tumors (adenoma and AD) and atypical adenomatous hyperplasia (a pretumor lesion) did not vary significantly between Dnmt3a-deficient and control animals at weeks 8 and 16 (Fig. 1*F* and Tables S1 and S2). These results suggest that Dnmt3a deficiency does not affect the initiation of K-ras–induced lung tumors but significantly promotes tumor growth.

Author contributions: Q.G. and R.J. designed research; Q.G., E.J.S., M.P., D.F., and S.R. performed research; Q.G., E.J.S., M.I.B., D.H., M.P., G.W.B., and R.J. analyzed data; and Q.G. and R.J. wrote the paper.

The authors declare no conflict of interest.

Data deposition: The microarray and methylation data reported in this paper have been deposited in the Gene Expression Omnibus (GEO) database, www.ncbi.nlm.nih.gov/geo (accession no. GSE32487).

[1]Present address: OralCDx Laboratories, Suffern, NY 10901.

[2]To whom correspondence should be addressed. E-mail: jaenisch@wi.mit.edu.

This article contains supporting information online at www.pnas.org/lookup/suppl/doi:10.1073/pnas.1114946108/-/DCSupplemental.

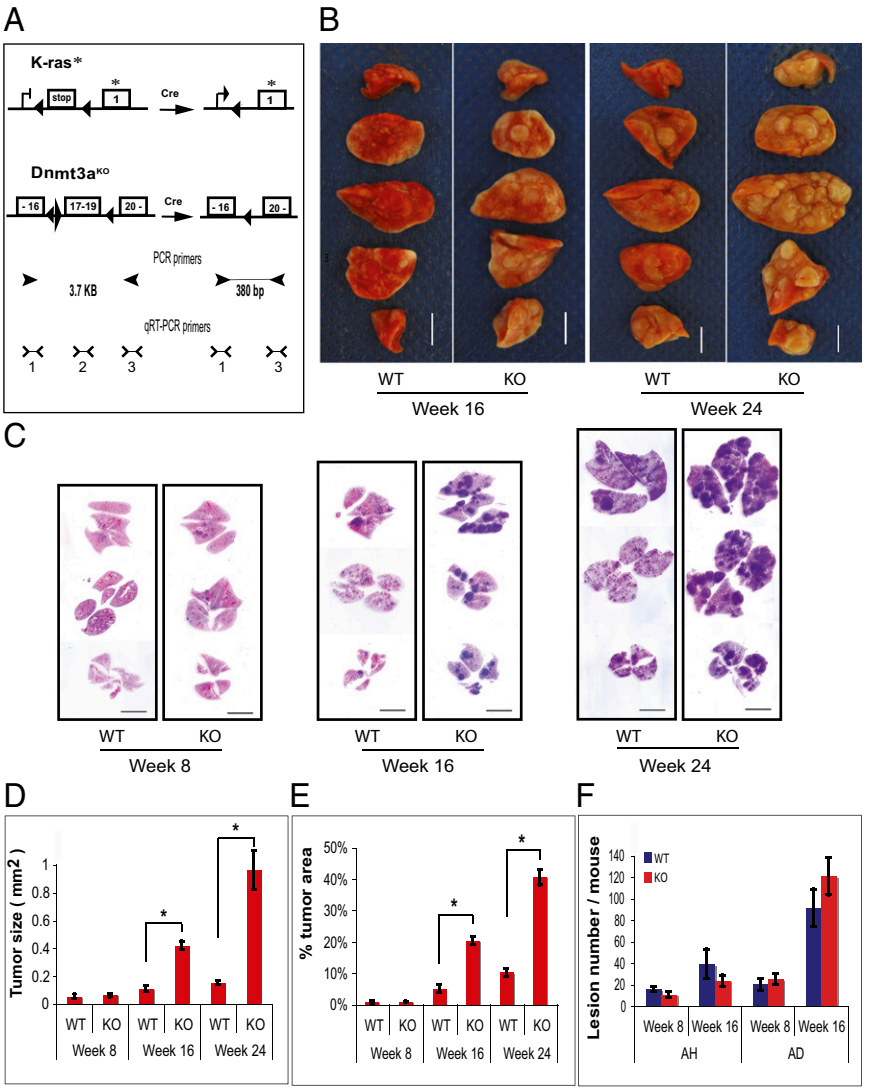

Fig. 1. Dnmt3a deficiency accelerates lung tumor growth in K-ras^{G12D} mice. (*A*) Schematic representation of the engineered locus in *K-ras* conditional knock-in and *Dnmt3a* conditional deletion mice before and after Cre-mediated recombination (modified from refs. 20 and 21). Positions of the PCR primers to detect recombination and the positions of three pairs of qRT-PCR primers to detect Dnmt3a mRNA expression are also indicated. stop, silencing element; boxed numerals indicate exon and its number. *G12D mutation; left-pointing black triangle indicates loxP site; right-pointing black triangle indicates frt site; arrowheads indicate PCR primers; > and < indicate qRT-PCR primers. (*B*) Tumors in lungs of Dnmt3a-deficient mice were significantly larger than those in Dnmt3a WT mice at weeks 16 and 24 after Ad-Cre infection. (Scale bar: 5 mm.) (*C*) Representative H&E-stained sections of lungs in Dnmt3a-deficient and WT mice at weeks 8, 16, and 24 after Ad-Cre infection. The tumors are seen as blue areas because of crowded nuclei stained blue by hematoxylin. Dnmt3a-deficient mice had an increased number of large tumors. (Scale bar: 6 mm.) (*D* and *E*) Comparison of tumor size (area) and fraction of lung area occupied by tumors. Both tumor size and tumor area fraction were significantly larger in Dnmt3a-deficient mice than in WT mice at weeks 16 and 24. *Comparisons that are significantly different. (Tumor size: wk 16, $P < 0.0001$; wk 24, $P = 0.0012$; tumor area fraction at weeks 16 and 24, $P < 0.0001$). (*F*) Comparison of number of tumor (adenoma and adenocarcinoma; AD) and atypical adenomatous hyperplasia (AH) at weeks 8 and 16. No significant difference was detected; $n = 4$ for both Dnmt3a KO and WT at weeks 8 and 24; $n = 5$ for both KO and WT mouse at week 16. Error bars indicate SEM.

Deletion of *Dnmt3a* in Tumors. To verify *Dnmt3a* deletion, we used PCR with primers flanking the Lox-P sites to detect recombination (Fig. 1*A*). Fig. 2*A* shows that all tumors tested had evidence for *Dnmt3a* deletion. This was confirmed by quantitative RT-PCR (qRT-PCR) using primers located 5′ to the deletion (primer pair 1), within the deletion (primer pair 2), and 3′ to the deletion (primer pair 3). Fig. 2*B* demonstrates that primer pairs 1 and 3 detected a relatively high level of mRNA whereas primer pair 2 generated a more than 10-fold lower signal in Dnmt3a-deficient tumors. This is consistent with efficient Cre-mediated deletion of exons 17 to 19, which encode essential residues of the catalytic center of Dnmt3a and with the production of a shortened Dnmt3a mRNA from the deletion allele. The low level of RNA detected in Dnmt3a-deficient tumors by primer pair 2 is likely caused by the presence of some stromal cells in the tumor samples.

To confirm that the deletion affects Dnmt3a protein expression, we performed immunohistochemical analyses on lung sections of Dnmt3a-deficient and WT mice by using an antibody that recognizes the aminoterminal region of the Dnmt3a protein. Fig. 2*C* shows strong nuclear as well as weak cytoplasmic staining in Dnmt3a WT tumors. In contrast, Dnmt3a-deficient tumors lacked nuclear staining and revealed only weak cytoplasmic immunoreactivity (Fig. 2*D*). This difference in staining pattern suggests that, although *Dnmt3a* mutant cells may produce low levels of truncated Dnmt3a protein, they do not express functional protein that can localize to the nucleus, and thus would be unable to methylate genomic DNA.

***Dnmt3a* Deletion Facilitates Tumor Progression and Shortens Lifespan.** To assess tumor progression and malignancy, we classified the tumors into three grades according to tumor differentiation (modified from ref. 23). Grade 1 tumors were well differentiated, and the tumor cells resembled type 2 pneumocytes with small round nuclei and granular cytoplasm. In contrast, grade 3 tumors represented poorly differentiated tumors with marked cellular and nuclear pleomorphism, high nucleus-to-cytoplasm ratio, prominent nucleoli, and numerous mitotic figures. Grade 2 tumors were moderately differentiated, with a degree of differentiation between those of grades 1 and 3. As summarized in Fig. 3*A*, a significantly higher fraction of tumors in Dnmt3a-deficient animals at weeks 16 and 24 after infection was of grades 2 and 3 compared with tumors in Dnmt3a WT mice (Tables S2 and S3).

We also evaluated the tumor growth pattern. Two types of tumor growth, a solid and a papillary growth pattern, can be distinguished in mouse lung tumor, with the papillary growth pattern being considered as characteristic for advanced tumors (24, 25). In solid tumors, tumor cells proliferate in a nest- or sheet-like fashion, whereas in papillary tumors, the cells grow

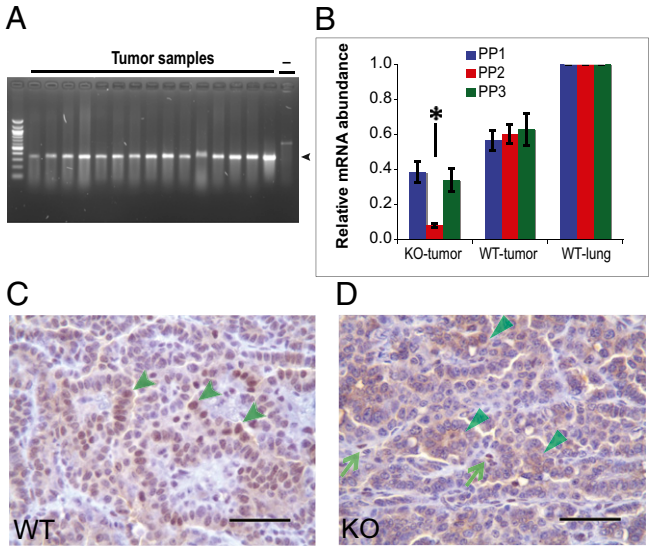

Fig. 2. Deletion and expression of *Dnmt3a*. (*A*) The targeted segment of *Dnmt3a* is deleted in Dnmt3a-deficient tumors. The expected 380-bp recombination bands (arrowhead) were detected in all tumors tested (40 tumors from nine Dnmt3a-KO mice). Dash indicates negative control. (*B*) Relative Dnmt3a mRNA abundance by qRT-PCR. Primer pairs (PP) 1 to 3 are located to the 5′ side, within, and to the 3′ side of the targeted deletion, respectively (Fig. 1*A*). Primer pair 2, which detects the segment removed in the deleted mRNA, gave a significantly lower signal (asterisk) in Dnmt3a-deficient tumors than those in normal lungs and WT tumors ($P < 0.0001$), indicating efficient deletion of the targeted segment. Primer pairs 1 and 3 detected a relatively high level of Dnmt3a mRNA in Dnmt3a-deficient tumors, suggesting production of a shortened Dnmt3a mRNA. Tumor numbers: KO, $n = 19$; WT, $n = 20$. Error bar indicates SEM. (*C* and *D*) Immunohistochemical staining for Dnmt3a protein with an Ab recognizing the aminoterminal region of Dnmt3a. In WT tumors (*C*), positive cells showed strong nuclear staining (indicated by arrowheads) with weak cytoplasmic signals, whereas in Dnmt3a-KO tumor cells (*D*), no typical nuclear signal was detected, with only occasional weak cytoplasmic staining (indicated by arrowheads). Strong nuclear signals were observed in 78 of 170 WT tumors ($n = 6$ mice) and no typical nuclear staining was detected in 160 Dnmt3a-KO tumors ($n = 6$ mice). Also note that some stromal cells in Dnmt3a-deficient tumor tissue display nuclear signals indicated by arrows (*D*). (Scale bar: 50 μm.)

around a fibrovascular core (Fig. 3*B*). Compared with the solid growth pattern, the papillary structure enables tumor cells to access blood circulation more efficiently, which is critical for tumor growth and progression. Fig. 3*B* shows that Dnmt3a-deficient mice had a significantly higher percentage of tumors with papillary structure (i.e., papillary tumors) at weeks 16 and 24 after infection than control mice (Tables S2 and S3). Finally, we observed tumor invasion in four Dnmt3a-deficient tumors (Fig. 3*C*), but no invasion was detected in WT tumors.

Consistent with the high tumor load and the more malignant tumor phenotype, the lifespan of Dnmt3a-deficient mice was significantly shorter than that of Dnmt3a heterozygous or WT mice (Fig. 3*D*). No significant difference was observed between Dnmt3a heterozygous and WT mice. Autopsies of approximately 70 animals revealed lung tumors as the most likely cause of death.

Dnmt3a-Deficient Tumors Have a High Proliferation Index. To investigate the possible basis of the accelerated growth of Dnmt3a-deficient tumors, we examined the cell proliferation and apoptosis indexes by immunostaining for proliferation marker Ki67 and apoptosis marker cleaved caspase-3. Fig. 4 *A*–*C* show that significantly more cells per unit area in Dnmt3a-deficient tumors were positive for Ki67 than in WT tumors, indicating that *Dnmt3a* mutant tumors were characterized by a higher proliferation index. In contrast, cells positive for cleaved caspase-3 were rare, and no significant difference was detected between Dnmt3a-deficient and WT tumors (Fig. 4*D*). These results suggest that the increased growth of Dnmt3a-deficient tumors is a result of increased proliferation rather than decreased apoptosis.

Gene Expression and DNA Methylation in Dnmt3a-Deficient Tumors. To gain insights into overall gene expression changes, we performed transcriptional profiling analyses by using whole mouse genome microarrays. A comparison between 12 pairs of Dnmt3a-deficient and WT tumors revealed that mRNA abundance of approximately 1,970 genes was significantly different between Dnmt3a-deficient and WT tumors [false discovery rate (FDR) < 0.05] with approximately 1,020 genes expressed at a higher and 940 genes expressed at a lower level in Dnmt3a-deficient tumors (Fig. 5*A* and Dataset S1). Gene Ontology enrichment analysis (26) revealed that the top three biological processes affected most significantly by these differentially expressed genes were blood vessel formation, cell adhesion, and regulation of cell motion (Fig. 5*B* and Dataset S1). These processes are key steps in cancer progression (27), consistent with the morphological findings that Dnmt3a-deficient tumors appear to be larger and more advanced. Also, no significant difference (using a raw *P* value threshold of 0.05) of the mRNA abundance was detected in Dnmt1 ($P = 0.46$) or Dnmt3b ($P = 0.34$) between Dnmt3a-deficient and WT tumors.

To examine whether Dnmt3a deficiency resulted in genomic methylation changes, we performed an unbiased methylome analysis. Methylated DNA isolated from three Dnmt3a-deficient and two WT tumors was immunoprecipitated and subjected to high-throughput sequencing [methylated DNA immunoprecipitation (MeDIP)-Seq], producing a total of 101 million reads. Because of the CpG density dependency of MeDIP, we only analyzed relative methylation levels comparing the two exact same regions in Dnmt3a-deficient and WT tumors. To identify differentially methylated regions (DMRs), we mapped the reads and scanned the genome in 1-kb windows with 100 bp overlap (*Materials and Methods*). We observed that 99.6% of the DMRs were less methylated in the Dnmt3a-deficient compared with the WT tumors (Table S4 and Dataset S2). Based on their overall distribution on the genome, a higher than expected percentage of less methylated regions overlapped gene bodies, particularly exons (Table S4). We further tested all genes and promoter regions for differential methylation (*Materials and Methods* and Dataset S2) and observed that genes that were less expressed in Dnmt3a-deficient tumors tended to have lower methylation levels in gene bodies (Fig. S1*A*). In contrast, gene expression changes did not correlate with promoter methylation (Fig. S1*B*). These results are consistent with a previous report showing a positive correlation between gene body methylation and gene expression in Dnmt3a-deficient neural cultures, suggesting that Dnmt3a-mediated nonpromoter methylation facilitates gene expression (28).

A previous study found methylation changes of repetitive sequences in established Dnmt3a mutant ES cells (29). We therefore performed Southern blot-based methylation assays to compare the DNA methylation status of minor satellite repeats and detected no obvious differences between Dnmt3a-deficient and WT tumors (Fig. S2). This suggests that Dnmt3a-dependent methylation changes of these sequences become manifest only after extensive cell passage and cell proliferation.

Discussion

The role of DNA methylation in the APC^{Min} model of intestinal tumors has been well established, with Dnmt3b deletion protecting against tumorigenesis and overexpression increasing tumor load by de novo methylation and silencing of tumor-suppressor genes (9, 10). In contrast, no role of Dnmt3a in

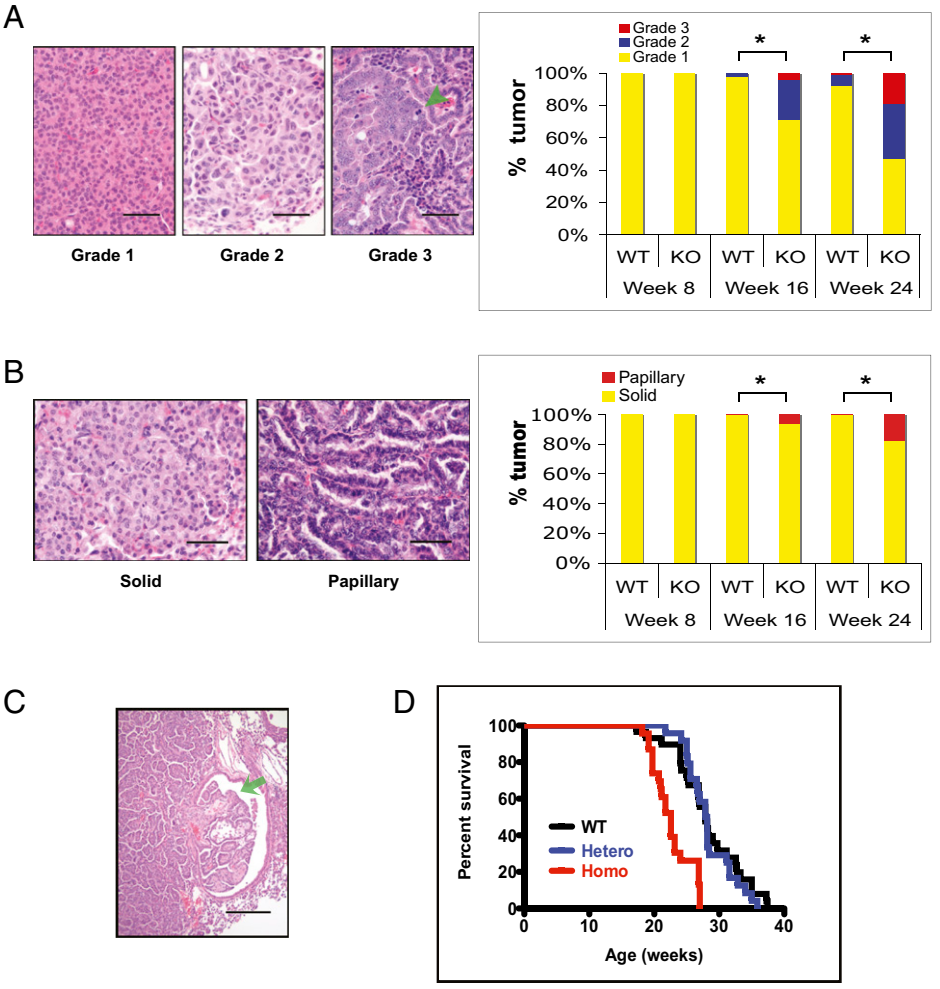

Fig. 3. Dnmt3a deficiency leads to more advanced tumors. (*A*) Dnmt3a-deficient mice had more grade 2 and grade 3 tumors than WT mice. Photomicrographs show the morphology of tumors of the three histological grades (arrowhead, mitotic figure). Bar graph demonstrates that Dnmt3a-deficient mice had a significantly higher percentage of grade 2 and 3 tumors at weeks 16 and 24 (week 16, $P = 0.0019$; week 24, $P < 0.0001$) and grade 3 tumors at week 24 ($P = 0.0034$). (*B*) Dnmt3a-deficient mice had more papillary tumors than WT mice. Photomicrographs show the morphology of solid and papillary growth pattern. Bar graph demonstrates that Dnmt3a-deficient mice had a significantly higher percentage of papillary tumors at weeks 16 and 24 (week 16, $P = 0.026$; week 24, $P = 0.0062$); $n = 4$ for Dnmt3a KO and WT at week 8 and 24; $n = 5$ for KO and WT mice at week 16. (*C*) Representative section showing invasion into a bronchiole (arrow) in a Dnmt3a-deficient tumor. (*D*) Dnmt3a-deficient (i.e., homozygous KO) mice have a significantly shorter lifespan than Dnmt3a heterozygous and WT mice ($P < 0.0001$). No significant difference was detected between Dnmt3a heterozygous and WT mice ($P = 0.63$). WT, Dnmt3a WT, $n = 29$; Homo, Dnmt3a homozygous KO, $n = 23$; Hetero, Dnmt3a heterozygous, $n = 24$. *Comparisons that are significantly different (at aforementioned P values). Photomicrographs show H&E staining. (Scale bars: *A* and *B*, 50 μm; *C*, 200 μm.)

APC^{Min} tumor formation has been established. Here we find that deletion of *Dnmt3a* promotes tumor growth and progression but not tumor initiation, suggesting that this gene, counter to expectation, acts like a tumor suppressor rather than like a cancer-promoting gene, as has been shown for Dnmt3b. Expression of genes involved in processes such as angiogenesis, cell adhesion, and cell motion was significantly altered in Dnmt3a-deficient tumors, consistent with an effect on tumor growth and progression.

The methylation status of DNA may affect cancer by several mechanisms: (*i*) global hypomethylation may increase genomic instability (3, 4), and (*ii*) hypermethylation of promoters can mediate tumor suppressor gene silencing (5, 9). However, the mechanism of how Dnmt3a affects gene expression and tumor formation is unclear. The genome of embryonic stem cells, in contrast to that of somatic cells, has methylated cytosine residues at non-CpG contexts, which has been suggested to result from the activity of Dnmt3a (30). More recently, whole-genome profiles of DNA methylation at single-base pair resolution of ES cells detected non-CpG methylation in gene bodies, which was positively correlated with gene expression (31). Another study demonstrated that Dnmt3a-dependent gene body methylation correlated with expression of genes involved in neural differentiation (28). Consistent with this observation, we found that gene bodies were less methylated in Dnmt3a-deficient tumors than in WT tumors, which also correlated with lower gene expression. Given that tumors in the mutant K-ras lung cancer model may arise from stem cells giving rise to more differentiated cells in the tumor (32), it is possible that Dnmt3a-dependent gene body methylation may be important for expression of genes that promote differentiation in a fraction of the tumor cells. Although mechanistic insights are lacking, our observation that Dnmt3a-deficient mice harbored more poorly differentiated and more advanced tumors is consistent with the notion that Dnmt3a deficiency interferes with the differentiation process in tumor cells, promoting the formation of less mature and more malignant tumors.

The majority of *DNMT3a* mutations found in myeloid neoplasm patients are missense mutations, and some of the mutations have been shown or predicted to result in reduced translation (14–16). However, because nearly all patients are heterozygous for the mutant allele it is not clear whether the *DNMT3a* mutations have dominant-negative effects or cause hemizygous insufficiency. In this context, our data using a *Dnmt3a*-null allele are of interest, as they argue against the possibility that hemizygous insufficiency affects lung tumors.

Based on the well established role of de novo DNA methylation-mediated gene silencing in cancer, inhibitors of methyltransferases are being actively investigated (33) and two drugs, azacitidine and decitabine, have been approved by the Food and Drug Administration for treatment of myelodysplastic syndrome (34, 35). Our data raise the possibility that such treatments, in addition to activating silenced tumor-suppressor genes, may have the unintended consequence of inhibiting DNMT3A, thereby affecting its proposed tumor-suppressor function. Therefore, it will be of great importance to elucidate the molecular mechanisms of how this gene affects cancer progression. The avail-

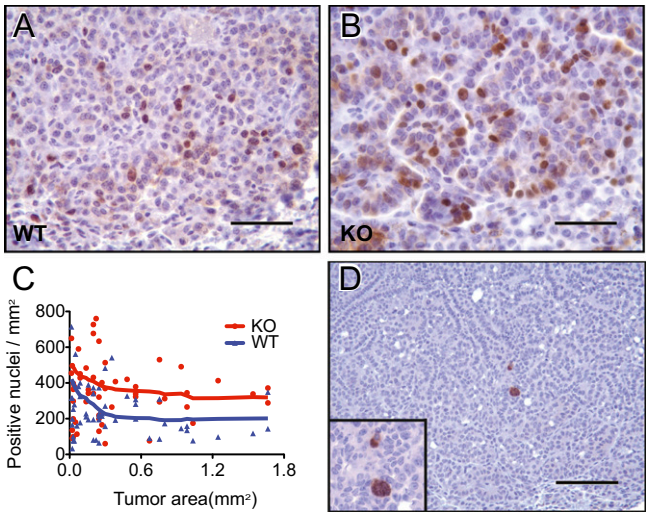

Fig. 4. Dnmt3a-deficient tumors have a higher proliferation index. (*A* and *B*) Representative photomicrographs of immunohistochemical staining for the proliferation marker K_i-67 in Dnmt3a WT (*A*) and KO mice (*B*). The positive signal localizes to the nuclei. (*C*) Plotting of proliferation index (positive nuclei/mm^2) against tumor size (mm^2). Dnmt3a-deficient tumors had a significantly higher proliferation index compared with WT tumors (P = 0.0006; the proliferation index was also influenced by tumor size, P = 0.032). (*D*) Representative photomicrograph of immunohistochemical staining for the apoptosis marker cleaved caspase-3 shows that positive cells are rare in Dnmt3a-deficient and WT tumors. (*Inset*) Details of two positive cells with cytoplasmic staining. (Scale bars: *A* and *B*, 50 μm; *C*, 200 μm.)

ability of a genetically defined experimental system will greatly facilitate these efforts.

Materials and Methods

Animal Models. *K-ras*$^{LSL\text{-}G12D}$ mice, which were provided by T. Jacks (Massachusetts Institute of Technology, Cambridge, MA) (20), were crossed with the Dnmt3a conditional KO mice (21) to generate mice with the following genotypes: *K-ras*$^{LSL\text{-}G12D/WT}$/*Dnmt3a*$^{2lox/2lox}$, *K-ras*$^{LSL\text{-}G12D/WT}$/*Dnmt3a*$^{WT/WT}$, and *K-ras*$^{LSL\text{-}G12D/WT}$/*Dnmt3a*$^{2lox/WT}$. After Ad-Cre–mediated recombination, mice were generated with lung cells that carried the *K-ras* mutation and were homozygous (i.e., KO), heterozygous, and WT at the *Dnmt3a* locus.

Ad-Cre (Gene Transfer Vector Core, University of Iowa) was delivered via an intratracheal approach (22). Briefly, 8- to 12-wk-old mice were anesthetized by i.p. injection of tribromoethanol (~0.4 mg/g body weight) and suspended on a bar of a mouse platform via their front teeth. A Fiber-lite Illuminator was used to illuminate the opening of the trachea, an i.v. catheter (22 gauge) was inserted into the trachea until the top of the catheter was near the mouse's front teeth, and 60 uL Ad-Cre (5×10^7 pfu in MEM containing 10 mM $CaCl_2$) was directly delivered into the catheter. In some of the microarray studies, we also used an intranasal infection approach. The procedure was similar to the intratracheal approach except that the virus was directly pipetted over the opening of one nostril of the mouse instead of delivering Ad-Cre via a catheter into the trachea.

Animal care was in accordance with institutional guidance and all animal studies were reviewed and approved by the Committee on Animal Care, Department of Comparative Medicine, Massachusetts Institute of Technology.

Mouse Examination, Tissue Preparation, and Histological Examination. For histological comparison, the mice were euthanized at weeks 8, 16, and 24 after Ad-Cre infection (no. of mice analyzed: week 8, Dnmt3a WT, n = 4; KO, n = 4; three pairs were littermates; week 16, WT, n = 5; KO, n = 5; four littermate pairs; week 24, WT, n = 4; KO, n = 4; three littermate pairs). During dissection, each organ was carefully examined with particular attention to mediastinal structures, especially lymph nodes. Any abnormal tissue was sampled for histological examination. The lungs were fixed by infusion of 10% formalin. After infiltrated by paraffin, the left lobe was trisected and the other lobes were bisected; they were then embedded in paraffin, sectioned (4 μm), and stained by H&E. Thus, each mouse's lungs were represented by 11 sections that were used for histopathological comparisons. In the survival study, mice were euthanized at end stage (mouse numbers: Dnmt3a WT, n = 29; homozygous, n = 23; heterozygous, n = 24). Before tissue fixation, representative lung tumors and normal tissue were flash-frozen in liquid nitrogen and stored at −80 °C for genomic DNA and RNA extraction. Tumor images were captured and analyzed by Pixel Link Capture SE (Pixel Link).

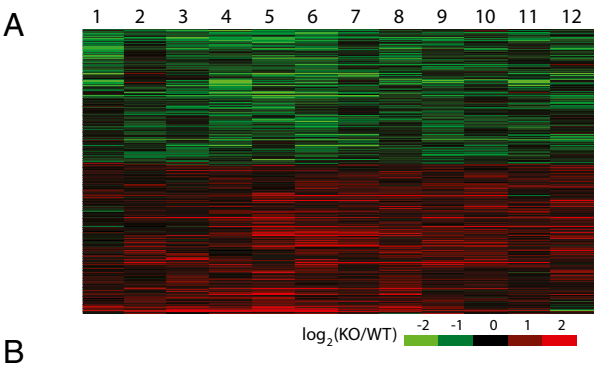

B

Cluster 1. Enrichment Score: 3.50

Process	GO id	Count	P Value
blood vessel morphogenesis	0048514	34	1.91E-04
blood vessel development	0001568	39	2.74E-04
angiogenesis	0001525	25	4.23E-04
vasculature development	0001944	39	4.47E-04

Cluster 2. Enrichment Score: 3.01

Process	GO id	Count	P Value
cell adhesion	0007155	75	1.58E-04
biological adhesion	0022610	75	1.68E-04
cell-cell adhesion	0016337	30	0.035

Cluster 3. Enrichment Score: 2.67

Process	GO id	Count	P Value
regulation of cell motion	0051270	22	2.94E-04
regulation of cell migration	0030334	17	0.005
regulation of locomotion	0040012	19	0.006

Cluster 4. Enrichment Score: 2.62

Process	GO id	Count	P Value
cellular macromolecule catabolic process	0044265	77	7.07E-04
modification-dependent macromolecule catabolic process	0043632	65	0.001
modification-dependent protein catabolic process	0019941	65	0.001

Cluster 5. Enrichment Score: 2.41

Process	GO id	Count	P Value
regulation of body fluid levels	0050878	19	5.34E-04
coagulation	0050817	16	8.09E-04
blood coagulation	0007596	16	8.09E-04

Cluster 6. Enrichment Score: 2.17

Process	GO id	Count	P Value
negative regulation of molecular function	0044092	30	2.24E-06
negative regulation of catalytic activity	0043086	23	4.20E-05
negative regulation of kinase activity	0033673	14	3.04E-04

Fig. 5. Gene expression in Dnmt3a-deficient and WT tumor. (*A*) Global expression profiling using whole mouse-genome microarrays. Heat map shows the top 1,967 differentially expressed genes between Dnmt3a-deficient and WT tumors (FDR < 0.05). Columns represent 12 matched KO/WT tumor pairs, and rows differentially expressed genes. (*B*) Gene enrichment analysis of the differentially expressed genes (FDR < 0.05) by the functional annotation tool in the Database for Annotation, Visualization, and Integrated Discovery using default thresholds. Shown are the top six clusters in biological process. Only the top three annotation terms are shown in cluster 4–6.

Immunohistochemistry. Immunohistochemistry was performed by using Vectastain Elite ABC kit (Vector) following the manufacturer's instructions, with the following primary antibodies: anti-Dnmt3a (sc-20703, 1:200 di-

MEDICAL SCIENCES

lution; Santa Cruz), anti–K_i-67 (clone TEC-3, 1:50 dilution; DakoCytomation), and anti–cleaved caspase-3 (no. 9661, 1:1,000 dilution; Cell Signaling). Dnmt3a staining was performed on 160 tumors in six Dnmt3a-deficient mice and 170 tumors in six WT mice. K_i-67 and cleaved caspase-3 staining were performed on 57 Dnmt3a-deficient tumors from two mice and 69 WT tumors from two mice.

PCR and RT-PCR. We used regular PCR to detect Cre-mediated recombination in tumors of *Dnmt3a* KO mice. The sequences of the PCR primes (Fig. 1*A*) were as follows: sense, 5′ggcttttcctcagacagtgg3′; antisense, 5′ tcaatcatcacggggttaga3′. PCR program was 95 °C for 2 min, 95 °C for 30 sec, 60 °C for 30 sec, 72 °C for 45 sec, 30 cycles; 72 °C for 6 min. Forty tumors with diameters from 0.1 cm to 0.4 cm were tested from nine *Dnmt3a*-KO mice. Genomic DNA (for large tumors) or tumor lysis (for small tumors) was used as template. Genomic DNA was isolated with AllPrep DNA/RNA mini kit (Qiagen). Lysis solution was proteinase K 0.5 mg/mL, 50 mM KCl, 10 mM Tris-HCl (pH 8.3), 2 mM $MgCl_2$, 0.1 mg/mL gelation, 0.45% Nonidet P-40, and 0.45% Tween 20.

The Dnmt3a mRNA abundance was analyzed in 19 tumors in four KO mice and 20 tumors in six WT mice by qRT-PCR. Three pairs of qRT-PCR primers were designed to detect Dnmt3a mRNA using primers located 5′ to the deletion (primer pair 1), within the deletion (primer pair 2), and 3′ to the deletion (primer pair 3). The primer sequences are as follows: primer pair 1, 5′ ggagccaccagaagaagaga3′, 5′gctctttctgggtttcttgg3′; primer pair 2, 5′ cctgcaatgacctctccatt3′, 5′cggccagtaccctcataaag3′; and primer pair 3, 5′gaacgagaggacggagaaaa3′, 5′tcctcctctgtggtttgctt3′. Total RNA was isolated with AllPrep DNA/RNA mini kit (Qiagen). First-strand cDNA was synthesized by SuperScript III First-Strand Synthesis SuperMix (Invitrogen). Real-time PCR was performed on 7900HT Fast Real-Time PCR System (Applied Biosystems) using SYBR Green Master (Roche), following manufacturer protocols. The expression data were analyzed by comparative C_T method.

Microarray. Total RNA was isolated from 12 matched Dnmt3a KO ~ WT tumor pairs from eight pairs of Dnmt3a KO ~ WT mice. Each pair of mice shared at least one parent. These 12 pairs of tumors included six pairs of large tumors (>0.4 cm in diameter) and six pairs of small tumors (<0.25 cm in diameter). The hybridization was performed on Agilent Whole Mouse Genome 4 × 44K microarrays (two-channel) by Whitehead Genome Technology Core.

The two-color microarray raw data were normalized across channels by loess (locally weighted scatter-plot smoothing, using spot quality weights) and between arrays by quantile normalization of average intensities ("Aquantile") using Bioconductor. Following summarization of replicate probes by median, differential expression was assayed by moderated *t* test and corrected for FDR, as implemented by the limma package in Bioconductor.

For gene enrichment analysis, we used the Database for Annotation, Visualization, and Integrated Discovery (26) to analyze the differentially expressed genes list between Dnmt3a-deficient and WT tumors (FDR < 0.05).

DNA Methylation Assays. MeDIP-seq was performed on three Dnmt3a-deficient and two WT tumors by using the Magmedip kit (Diagenode) according to the manufacturer's protocol. Libraries were sequenced on the genome analyzer II (Illumina). Data analysis was similar to that described by Bock et al. (36).

Details of MeDIP-Seq and Southern blot analysis are provided in *SI Materials and Methods*.

Statistical Analysis. We used Prism 5 (GraphPad Software) to perform statistical analysis, with two-tailed Student *t* test for the comparison of tumor number, size, grade, growth pattern, invasion, and fraction of tumor area; Kaplan–Meier survival analysis for comparison of lifespan; and two-way ANOVA for comparison of proliferation and apoptosis indexes. Unless indicated otherwise, 0.05 was used as the *P* value threshold for statistical significance.

ACKNOWLEDGMENTS. We thank J. Dausman, R. Flannery, and K. Ganz for maintenance of the mouse colony and F. Soldner, L. Medeiros, G. Welstead, S. Sarkar, D. Faddah, and Y. Buganim for helpful discussions and critical comments on the manuscript. We thank T. Jacks (Massachusetts Institute of Technology) for providing K-ras mutant mice and A. Cheung and A. Dooley for technical assistance on intratracheal virus delivery. We also thank B. Yuan, R. Bronson, and D. Crowley for advice in statistics or histopathology; D. Cook, A. Leshinski, and C. Whittaker for running the Solexa pipeline; and J. Kwon, J. Love, and S. Gupta for performing microarray hybridization. This work was supported by a grant from Philip Morris International and National Institutes of Health Grant R01-CA087869.

1. Feinberg AP (2007) Phenotypic plasticity and the epigenetics of human disease. *Nature* 447:433–440.
2. Jones PA, Baylin SB (2007) The epigenomics of cancer. *Cell* 128:683–692.
3. Gaudet F, et al. (2003) Induction of tumors in mice by genomic hypomethylation. *Science* 300:489–492.
4. Chen RZ, Pettersson U, Beard C, Jackson-Grusby L, Jaenisch R (1998) DNA hypomethylation leads to elevated mutation rates. *Nature* 395:89–93.
5. Sharma S, Kelly TK, Jones PA (2010) Epigenetics in cancer. *Carcinogenesis* 31:27–36.
6. Okano M, Xie S, Li E (1998) Cloning and characterization of a family of novel mammalian DNA (cytosine-5) methyltransferases. *Nat Genet* 19:219–220.
7. Mizuno S, et al. (2001) Expression of DNA methyltransferases DNMT1, 3A, and 3B in normal hematopoiesis and in acute and chronic myelogenous leukemia. *Blood* 97: 1172–1179.
8. Nosho K, et al. (2009) DNMT3B expression might contribute to CpG island methylator phenotype in colorectal cancer. *Clin Cancer Res* 15:3663–3671.
9. Linhart HG, et al. (2007) Dnmt3b promotes tumorigenesis in vivo by gene-specific de novo methylation and transcriptional silencing. *Genes Dev* 21:3110–3122.
10. Lin H, et al. (2006) Suppression of intestinal neoplasia by deletion of Dnmt3b. *Mol Cell Biol* 26:2976–2983.
11. Steine EJ, et al. (2011) Genes methylated by DNA methyltransferase 3b are similar in mouse intestine and human colon cancer. *J Clin Invest* 121:1748–1752 10.1172/JCI43169.
12. Robertson KD, et al. (1999) The human DNA methyltransferases (DNMTs) 1, 3a and 3b: Coordinate mRNA expression in normal tissues and overexpression in tumors. *Nucleic Acids Res* 27:2291–2298.
13. Deng T, et al. (2009) An essential role for DNA methyltransferase 3a in melanoma tumorigenesis. *Biochem Biophys Res Commun* 387:611–616.
14. Ley TJ, et al. (2010) DNMT3A mutations in acute myeloid leukemia. *N Engl J Med* 363: 2424–2433.
15. Yan XJ, et al. (2011) Exome sequencing identifies somatic mutations of DNA methyltransferase gene DNMT3A in acute monocytic leukemia. *Nat Genet* 43:309–315.
16. Walter MJ, et al. (2011) Recurrent DNMT3A mutations in patients with myelodysplastic syndromes. *Leukemia* 25:1153–1158.
17. Jemal A, Siegel R, Xu J, Ward E (2010) Cancer statistics, 2010. *CA Cancer J Clin* 60: 277–300.
18. Brock MV, et al. (2008) DNA methylation markers and early recurrence in stage I lung cancer. *N Engl J Med* 358:1118–1128.
19. Belinsky SA (2004) Gene-promoter hypermethylation as a biomarker in lung cancer. *Nat Rev Cancer* 4:707–717.
20. Jackson EL, et al. (2001) Analysis of lung tumor initiation and progression using conditional expression of oncogenic K-ras. *Genes Dev* 15:3243–3248.
21. Nguyen S, Meletis K, Fu D, Jhaveri S, Jaenisch R (2007) Ablation of de novo DNA methyltransferase Dnmt3a in the nervous system leads to neuromuscular defects and shortened lifespan. *Dev Dyn* 236:1663–1676.
22. DuPage M, Dooley AL, Jacks T (2009) Conditional mouse lung cancer models using adenoviral or lentiviral delivery of Cre recombinase. *Nat Protoc* 4:1064–1072.
23. Jackson EL, et al. (2005) The differential effects of mutant p53 alleles on advanced murine lung cancer. *Cancer Res* 65:10280–10288.
24. Nikitin AY, et al. (2004) Classification of proliferative pulmonary lesions of the mouse: Recommendations of the mouse models of human cancers consortium. *Cancer Res* 64: 2307–2316.
25. Renne R, et al. (2009) Proliferative and nonproliferative lesions of the rat and mouse respiratory tract. *Toxicol Pathol* 37(suppl):5S–73S.
26. Huang W, Sherman BT, Lempicki RA (2009) Systematic and integrative analysis of large gene lists using DAVID bioinformatics resources. *Nat Protoc* 4:44–57.
27. Talmadge JE, Fidler IJ (2010) AACR centennial series: The biology of cancer metastasis: Historical perspective. *Cancer Res* 70:5649–5669.
28. Wu H, et al. (2010) Dnmt3a-dependent nonpromoter DNA methylation facilitates transcription of neurogenic genes. *Science* 329:444–448.
29. Liang G, et al. (2002) Cooperativity between DNA methyltransferases in the maintenance methylation of repetitive elements. *Mol Cell Biol* 22:480–491.
30. Ramsahoye BH, et al. (2000) Non-CpG methylation is prevalent in embryonic stem cells and may be mediated by DNA methyltransferase 3a. *Proc Natl Acad Sci USA* 97: 5237–5242.
31. Lister R, et al. (2009) Human DNA methylomes at base resolution show widespread epigenomic differences. *Nature* 462:315–322.
32. Kim CF, et al. (2005) Identification of bronchioalveolar stem cells in normal lung and lung cancer. *Cell* 121:823–835.
33. Belinsky SA, et al. (2011) Combination therapy with vidaza and entinostat suppresses tumor growth and reprograms the epigenome in an orthotopic lung cancer model. *Cancer Res* 71:454–462.
34. Taby R, Issa JP (2010) Cancer epigenetics. *CA Cancer J Clin* 60:376–392.
35. Rodríguez-Paredes M, Esteller M (2011) Cancer epigenetics reaches mainstream oncology. *Nat Med* 17:330–339.
36. Bock C, et al. (2010) Quantitative comparison of genome-wide DNA methylation mapping technologies. *Nat Biotechnol* 28:1106–1114.